Improving Separation Efficiency in End-of-Life Lithium-Ion Batteries Flotation Using Attrition Pre-Treatment

Anna Vanderbruggen [1,2,*] , Aliza Salces [1] , Alexandra Ferreira [3] , Martin Rudolph [1] and Rodrigo Serna-Guerrero [2]

[1] Helmholtz Zentrum Dresden Rossendorf (HZDR), Helmholtz Institute Freiberg for Resource Technology (HIF), Chemnitzer Straße 40, 09599 Freiberg, Germany; a.salces@hzdr.de (A.S.); m.rudolph@hzdr.de (M.R.)

[2] Department of Chemical and Metallurgical Engineering, School of Chemical Engineering, Aalto University, 2150 Espoo, Finland; rodrigo.serna@aalto.fi

[3] Laboratoire GeoRessources, Université de Lorraine, CNRS, F-54000 Nancy, France; alexandra.ferreira-desroix@univ-lorraine.fr

[*] Correspondence: a.vanderbruggen@hzdr.de

Abstract: The comminution of spent lithium-ion batteries (LIBs) produces a powder containing the active cell components, commonly referred to as "black mass." Recently, froth flotation has been proposed to treat the fine fraction of black mass (<100 μm) as a method to separate anodic graphite particles from cathodic lithium metal oxides (LMOs). So far, pyrolysis has been considered as an effective treatment to remove organic binders in the black mass in preparation for flotation separation. In this work, the flotation performance of a pyrolyzed black mass obtained from an industrial recycling plant was improved by adding a pre-treatment step consisting of mechanical attrition with and without kerosene addition. The LMO recovery in the underflow product increased from 70% to 85% and the graphite recovery remained similar, around 86% recovery in the overflow product. To understand the flotation behavior, the spent black mass from pyrolyzed LIBs was compared to a model black mass, comprising fully liberated LMOs and graphite particles. In addition, ultrafine hydrophilic particles were added to the flotation feed as an entrainment tracer, showing that the LMO recovery in overflow products is a combination of entrainment and true flotation mechanisms. This study highlights that adding kerosene during attrition enhances the emulsification of kerosene, simultaneously increasing its (partial) spread on the LMOs, graphite, and residual binder, with a subsequent reduction in selectivity.

Keywords: black mass; spent lithium-ion batteries; graphite; lithium metal oxides; froth flotation; mineral processing; recycling

1. Introduction

Lithium-ion batteries (LIBs) are the key technology to electrify transportation, which is one of the multiple measures proposed to prevent global warming [1]. With its dominant application in electric mobility, the global battery demand is forecast to increase 14-fold by 2030 from 2018 levels, consequently driving the demand for battery materials such as Co, Li, Ni, and graphite [2]. Mining and recycling will play an important role in fulfilling the demand for battery materials and ensuring the sustainability of the battery supply chain. Most importantly, spent LIBs should not be landfilled according to the Battery Directives (2006/66/EC; 2008/98/EC) due to their heavy metal contents, which pollute the land and groundwater. Furthermore, the residual energy of spent LIBs can trigger explosions, fire, and the release of toxic gases. The current and emerging recycling technologies focus on the recovery of LIB components that have high economic value such as Co, Ni, and Cu. Currently, pyrometallurgy is the main route utilized to recover valuable metals from spent LIBs. In pyrometallurgy, the spent LIBs are directly fed to the smelting furnace (>1000 °C) to

recover Co, Ni, and Cu, while graphite is used as a reducing agent and significant amounts of Al and Li are lost in slag [3]. Hydrometallurgy is a low-energy process and is seen as a potential solution to recover more active materials compared to the pyrometallurgy process [4,5]. In this process, LIBs are mechanically prepared by shredding and sieving to obtain the "black mass", which contains the electrode components such as lithium metal oxides (LMOs) and graphite. Organic acid (i.e., citric and succinic acid), inorganic acid (hydrochloric, sulfuric and nitric acid), and microorganisms can be used as reagents to selectively dissolve target metals [6]. Nevertheless, these recycling processes only recover a fraction of LIB components which, in compliance with the new EU battery regulation, will need to attain recycling efficiencies of 65% by average weight by 2025 and 70% by 2030 [7].

According to Asenbauer et al. [8], "graphite is and will remain to be an essential component of commercial lithium-ion batteries in the near- to mid-term future—either as sole anode active material or in combination with high-capacity compounds such as under stoichiometric silicon oxide, silicon–metal alloys, or elemental silicon". In typical commercial LIBs, graphite comprises 15–20% of its weight [9], making it a strategic candidate to meet the increasing recycling efficiencies. Natural graphite, particularly in its spherodized form, is also categorized as a critical material in the EU, Canada, and Australia as a result of the supply risk for its production, which is at the moment is almost exclusively produced by China [10,11]. Thus, properly designed processes for the recovery of graphite from LIBs would result in a diversification of the graphite supply for Europe. In addition, the removal of graphite from the black mass is also beneficial for subsequent metallurgical processing. In pyrometallurgy, the high content of carbon can result in excessive CO_2 emissions and affects the operating conditions such as the CO_2/CO ratio, reaction kinetics, and melt properties, and consequently, the metal recovery and process efficiency [12]. In hydrometallurgy, the removal of graphite minimizes the feed material volume, thus reducing the consumption of water and reagents. The leaching process can also pollute and/or deteriorate graphite, and thus may not be suitable for the upcycling of spent anode materials [13].

Previous studies have recommended the use of froth flotation, which can be applied to the fine fraction of the black mass (<100 μm) to separate the graphite particles from the lithium metal oxides (LMOs) into two valuable products, increasing the overall efficiency of LIB recycling [14–16]. It has even been claimed that after separation through mechanical means, the LMOs [17,18] and graphite particles [19,20] can be applied for battery remanufacturing. Froth flotation, a separation process based on surface wettability, is one of the most common processes currently used for primary resource beneficiation [21,22], however, it is still an emerging technique for black mass beneficiation. The concept of froth flotation as a separation technique for active cell components was introduced as early as 2003 based on the assumption of the contrasting surface wettabilities of graphite and LMOs [14]. Many studies have emphasized that the presence of an organic binder coating the active components complicates the separation process and remains among the biggest challenges in black mass flotation [14,23]. Consequently, various pre-treatment strategies have been studied to remove the coated binder before flotation. Mechanical grinding [24] has been applied to the black mass before flotation, reportedly resulting in a high LMO grade of 97.2% in the underflow product with a low recovery of 49.3%. In another study, a Fenton reagent pre-treatment proved to be effective in removing the binder, but led to the formation of hydrophobic Fenton secondary products on the surfaces of the LMOs, resulting in the separation of LMOs with a high grade [25,26]. Other researchers have claimed that the application of pyrolysis between 400 °C and 600 °C decomposes the binder and improves the flotation efficiency [14,15,27–29]. For instance, Zhang et al. [29] applied mechanical crushing followed by a pyrolysis stage at 500 °C with a heating rate of 10 °C/min and pyrolysis time of 15 min, finally floating the fine fraction of the pyrolyzed product. Reportedly, with a rougher flotation stage, the underflow product obtained had a grade of 94.7% LMOs with a recovery of only 83.7%.

Another challenge in black mass flotation is the fine particle sizes of the liberated active components that have a typical D_{50} of ca. 15 μm, which are highly prone to entrainment. En-

trainment is the non-selective mechanical transfer of materials from the pulp to froth layer, directly affecting the grade of hydrophobic products [30]. The recovery by entrainment in froth flotation is well documented and strongly related to the recovery of water [31–34] and other operating factors such as pulp density, material density, froth height, and airflow [30]. It is also worth noting that entrainment may not be the only mechanism of LMO recovery in black mass flotation. Vanderbruggen et al. [35] recently reported that LMOs without a coated binder could attach to an air bubble and also interact with kerosene.

Bearing the aforementioned challenges in mind, the present study aimed to enhance the separation efficiency of pyrolyzed black mass by applying a high shear (i.e., attrition) pre-treatment before flotation in order to remove the residual coated binder. This concept is inspired by high-intensity conditioning (HIC), which is used in the flotation of coal, graphite, and other minerals [36–39] to improve the flotation efficiency by de-aggregating particles, removing the slime coating, and reactivating mineral surfaces. Furthermore, the addition of kerosene during HIC can result in better emulsification and dispersion of oil droplets, leading to an enhanced collision probability with solid particles and improved flotation kinetics, as demonstrated by Zhou et al. [40] in their work on graphite ore. Therefore, it is of interest in this work to investigate the most efficient strategy for kerosene addition either during or after attrition pre-treatment.

Unlike the majority of published works aimed at black mass flotation where the focus has been on the recovery of cathode materials, the present work is interested in both the LMOs and graphite. Evidently, this can only be achieved by understanding the flotation mechanisms present in this system of mixed materials. Consequently, experimental work was carried out to assess the impact of the two aspects above-mentioned on affecting the quality of the black mass flotation products, namely, the presence of residual binder and the entrainment of fine particles. For the former, flotation results of an industrial pyrolyzed black mass sample containing a residual binder were compared to a model black mass used as a benchmark. The model black mass consisted of a mixture of pristine graphite and LMO particles, thus binder-free. To address the latter, fine hydrophilic particles were added to the black mass as an entrainment tracer to understand the contribution of this flotation mechanism.

2. Materials and Methods

2.1. Samples and Reagents

For this study, a black mass sample was provided by an industrial scale operator, Accurec Recycling GmbH. The spent LIBs were sorted at the plant by chemistry, and a mixture of nickel-manganese-cobalt oxides (NMCs) and lithium cobalt oxides (LCOs) were used as a feed for this recycling process. The black mass received underwent a vacuum pyrolysis treatment at 500–600 °C, followed by dry crushing and sieving. The fraction sieved below 100 μm was used for the flotation tests and its chemical composition determined by X-ray fluorescence (XRF) and C assay (described in Section 2.3) is given in Figure 1. In the fine fraction of this black mass, each chemical element can be associated with a special battery component: the graphite particles made of C; lithium metal oxides made of Co, Ni, Mn, and Li; cathode current collector made of Al; anode current collector made of Cu; and the casing particles mainly made of Fe. It should be highlighted that the content of Al, Cu, and Fe in the spent black mass highly depends on the comminution (liberation) stage of the recycling process. In the recycling industry, the cells are usually opened by comminution processes, leading to the production of fine particles [18] as opposed to manual dismantling in laboratory studies. Hence, there is a high probability of finding foil particles in the fine fraction of industrial black mass (below 100 μm), as shown by the characterization of the industrial black masses of Ruismäki et al. [41] or Vanderbruggen et al. [42].
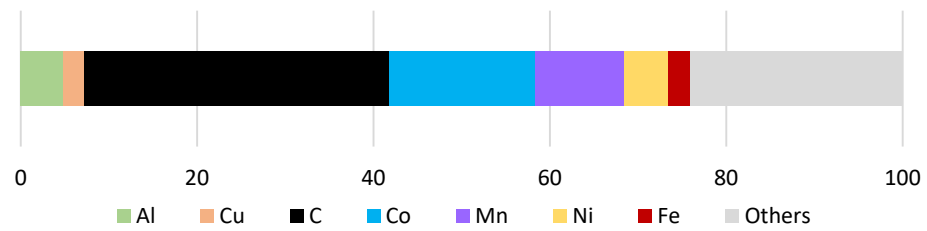
Figure 1. Chemical composition of the spent black mass by XRF and C assay. The group "Others" corresponds to the elements below 1 wt.% content and light elements excluding C such as Li, O, and F.

To understand the influence of the spent components and residual binder on black mass flotation, tests were also performed on a model black mass consisting of fully liberated and binder-free active particles. This model black mass was prepared by mixing pristine lithium metal oxides $LiNi_{0.33}Mn_{0.33}Co_{0.33}O_2$ (NMC-111, MSE supplies, Product No. PO0126) and spheroidized natural graphite (ProGraphite GmbH, product No. 1112-1) in a ratio of 60:40.

In addition, to estimate the degree of entrainment during black mass flotation, ultrafine glass spheres (Omicron® NP5-P0, Sovitec) were added as an entrainment tracer to the flotation feed, representing 6.4% by weight. These particles are considered hydrophilic and had the following nominal PSD: D_{10}, D_{50}, D_{90} of 0–3 μm 5–9 μm 12–16 μm, respectively. For the flotation tests, two reagents were used with fixed dosage. Escaid™ 110 from ExxonMobil (Hydrocarbon fluid, Product No. 20171206) was used at a dosage of 350 g/t as the promoter (collector) to enhance the natural hydrophobicity of graphite surfaces. Methyl isobutyl carbinol (MIBC) supplied by Alfa Aesar (99% $C_6H_{14}O$, Product No. A13435) was used as a frother with a dosage of 150 g/t.

2.2. Froth Flotation

The batch flotation tests were conducted in a laboratory-scale mechanically stirred cell GTK Labcell from Outotec with automatic scraping, using a 1.6 L capacity cell. Three conditioning strategies were tested in this study, as illustrated in Figure 2:

- No attrition pre-treatment (I);
- Attrition pre-treatment (II); and
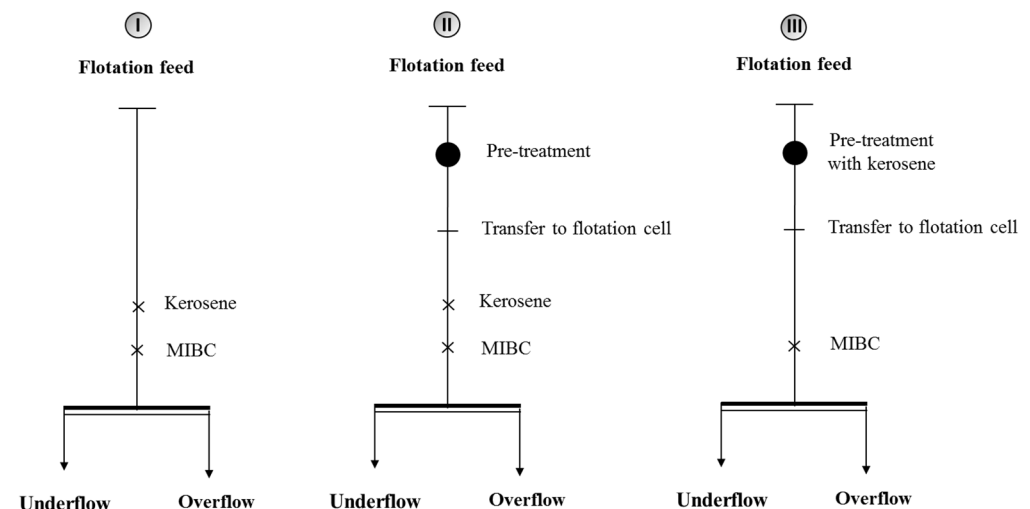- Attrition pre-treatment with kerosene addition (III).

Figure 2. The three flow diagrams for the flotation experiments. (**I**) No pre-treatment, (**II**) With pre-treatment, (**III**) Kerosene added during the pre-treatment.

It is worth noting that in the present study, the flotation products are referred to as "overflow" and "underflow" as opposed to the commonly used terms of "concentrate" and "tailings" used in froth flotation. This is because tailings is a term implying waste, but in the case of back mass separation, valuable anode and cathode materials are enriched into the froth and dispersed phases, respectively.

For (I), the sample was directly dispersed with tap water (6.5% solid) in the flotation cell using an impeller speed of 1000 min^{-1}. After 2 min of agitation, conditioning with kerosene was carried out for 3 min followed by MIBC for 1 min. In addition, one flotation test was carried out as (I) without kerosene to estimate the influence of this reagent.

For (II), the black mass sample was dispersed at 40% solid content in water and mixed at 16,000 min^{-1} using an Ultra Turrax high shear mixer (IKA, dispersing unit S25N−25F, Königswinter, Germany). After 10 min of pre-treatment, the slurry was transferred to the flotation cell with additional water to reach the same pulp density as in (I) and followed the same conditioning procedure with kerosene and MIBC.

For (III), kerosene was added during the attrition pre-treatment stage instead of adding it in the flotation cell. The conditions during pre-treatment were the same as in (II). After 10 min of pre-treatment, the slurry was transferred to the flotation cell such as in (I) and agitated for 2 min, followed with MIBC conditioning for 1 min.

The percent solids, reagent dosage, impeller speed, and airflow rate were constant for all experiments (I, II, and III) and were 6.5% solid, 350 g/t kerosene, and 150 g/t MIBC at 1000 min^{-1} and 4 L·min^{-1}. Five overflow products were collected to study the kinetics with the following collection times: C1 =18 s, C2 = 36 s, C3 = 54 s, C4 = 90 s, and C5 = 390 s. The times used for the kinetic study were based on previous test experiments.

After each flotation experiment, the mass of the five overflow products was measured before and after drying to determine the mass pull and the water pull. Drying was performed in an oven under natural convection for 12 h at 45 °C. Finally, representative dry samples were prepared for characterization. The flotation recoveries were calculated using Equation (1).

$$R(i) == \frac{C \cdot c(i)}{F \cdot f(i)} \tag{1}$$

where R is the recovery of the component i; C is the overflow product mass; c is the grade of the element i in the overflow product; F is the feed mass; and f is the grade of component i in the feed.

To assess the contribution of true flotation and entrainment to the recovery of LMO particles, the degree of entrainment (ENT) was estimated by using tracer particles. These particles are fully liberated and fine hydrophilic particles, therefore assumed to be recovered only by entrainment mechanisms. ENT for the tracer particles is calculated as the ratio of the mass of tracer particles per unit mass of water in the overflow product (Johnson, 1972 [43]). Equation (2) is used to calculate the degree of entrainment:

$$ENT(tracer, t) = \frac{R(tracer, t)}{W(t)} \tag{2}$$

where $R(tracer,t)$ is the recovery of tracer particles at a certain time in the overflow product and $W(t)$ is the water pull at the same time. The contribution of entrainment in the flotation of LMOs can thus be determined by a comparison of $ENT(tracer,t)$ with the total recovery per volume of water "R/W", which includes all possible flotation mechanisms.

2.3. Characterization

The particulate and compositional characteristics of the flotation feed and products were visualized by a scanning electron microscope (SEM, FEI Quanta 600 F) equipped with a field emission source (FEG) and an SSD-EDS X-ray spectrometer (Bruker Quantax X-Flash 5030 EDS-Detectors). The loose powder samples were fixed on a tab (PELCO Tabs TM, 6 mm OD from TED PELLA, INC, Redding, CA, USA). In this study, the backscattered

electron (BSE) image and secondary electron (SE) image were superimposed and false colors were attributed to generating an image with compositional, textural, and topographic information. The BSE signal intensity is governed by the density (by means of the atomic number (Z)) of the particles and shows a contrast in elemental composition between each particle. The blue color was imposed for high density, highlighting the LMO particles made of heavy metals, and black color for low density, highlighting the graphite and binder particles. The SE signal is sensitive toward the topography of the substrate surface and is highlighted through orange colors.

The samples were analyzed using an X-ray fluorescence (XRF), (NitonTM XL3t 980, Thermo Scientific, Waltham, MA, USA), with an end-window X-ray tube with a gold-anode and a voltage of 8 kV to 50 kV. The carbon content was analyzed by ALS laboratories in Ireland. The procedure consists of leaching with dilute hydrochloric acid to remove inorganic carbon. After filtering, washing, and drying, the remaining sample residue was roasted at 425 °C to remove the organic carbon. The roasted residue was later analyzed for carbon in a high-temperature LECO furnace with infrared detection.

To analyze the effect of pre-treatment on PSD, a sample was taken before and after the 10 min pre-treatment and analyzed by laser diffraction (HELOS with RHODOS dry deagglomeration by Sympatec HELOS GmbH, Clausthal-Zellerfeld, Germany). The measurements were conducted in triplicate.

3. Results and Discussion

3.1. Flotation Trends of Spent Black Mass

For the beneficiation of spent black mass, the graphite and metal oxide particles can be separated by froth flotation. As detailed in Section 2.2, three different conditioning procedures were applied, each resulting in distinctive separation efficiencies. The grade-recovery curves of graphite and metallic components in the overflow product are shown in Figures 3 and 4, respectively.
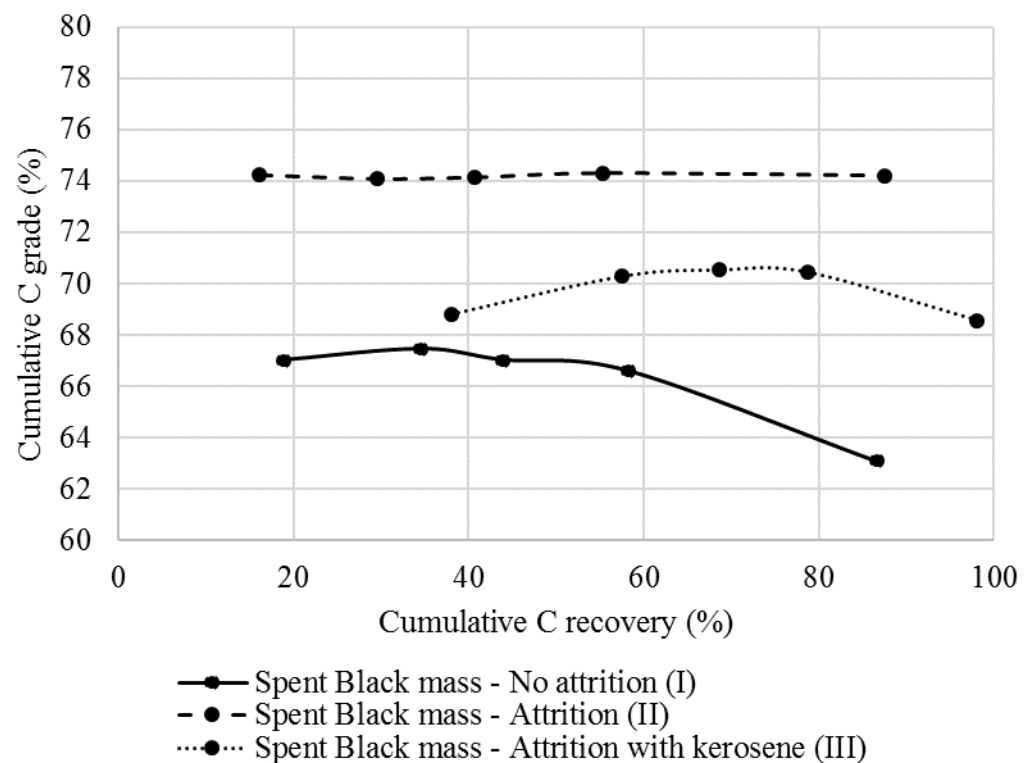

Figure 3. Grade and recovery of carbon in the overflow product according to the flotation flow: no attrition (**I**), with attrition (**II**), and attrition with kerosene (**III**).
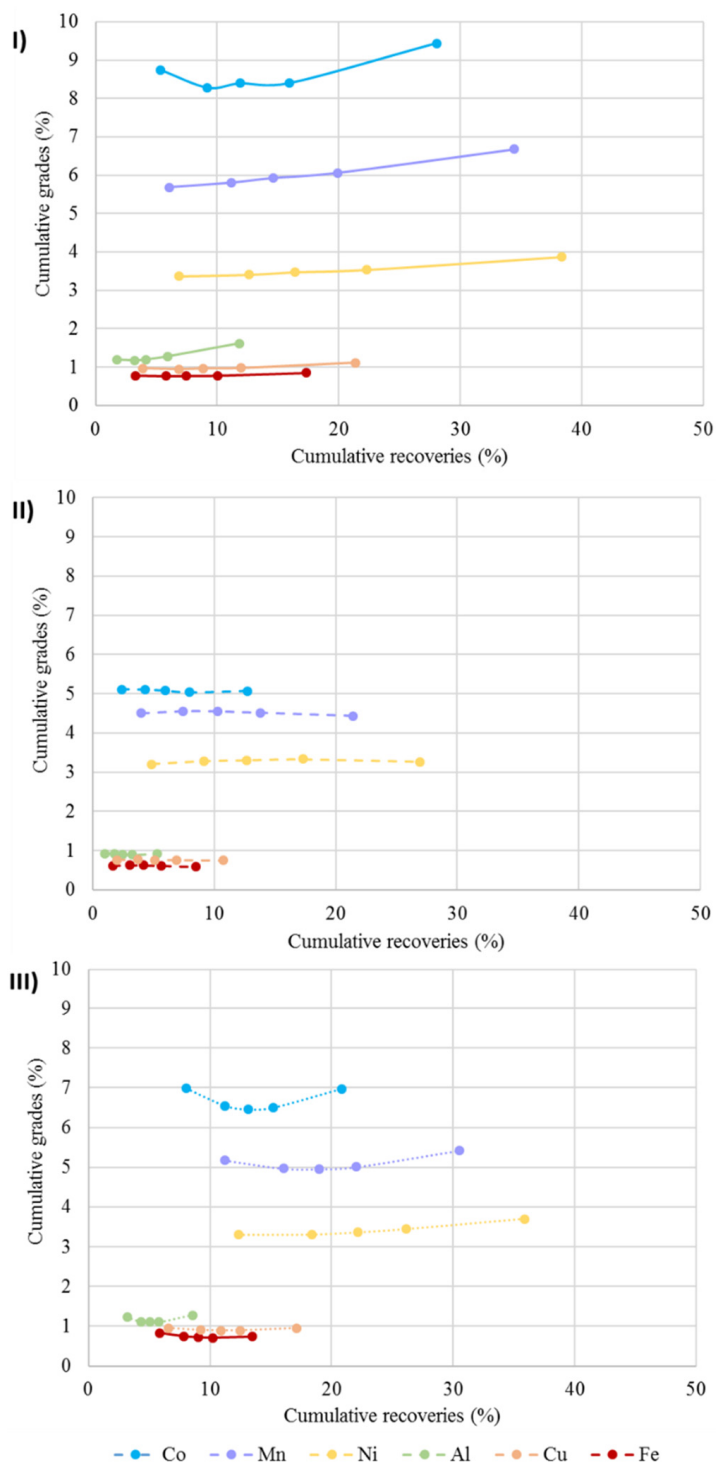
Figure 4. Grade recoveries of the impurities in the overflow products during spent black mass flotation. (**I**) No attrition, (**II**) With attrition, (**III**) Attrition with kerosene.

The mass pull obtained without pre-treatment (I) was 47.5%, but when attrition was applied (II), the mass pull dropped to 40.5%. This is likely associated with a more efficient separation since the grade of C in the overflow product increased from 63.1% to 74.2% (Figure 3). Nevertheless, the final graphite recovery for (I) and (II) were similar at 86.6% and 87.5%, respectively (Figure 3). Furthermore, to highlight the necessity of kerosene for spent graphite flotation, a test without kerosene and with only MIBC was carried out. This test resulted in a low mass pull of 12% and only 31% graphite recovery in the overflow product,

leading to low separation efficiency. However, in a previous study from our group [35], pristine spheroidized graphite was floated with a 90% recovery under similar conditions in the absence of kerosene. These results point out that the hydrophobicity of spent graphite is lower than fresh spheroidized graphite, possibly due to residual binder or a solid electrolyte interphase (SEI) layer partially removed during pyrolysis [13]. A collector is thus required to sufficiently enhance the hydrophobicity of spent graphite before flotation.

It is noteworthy that the grade of graphite in the overflow product did not follow the typical trend in flotation where it decreased as recovery increased. As seen in this study, the grade/recovery trends observed showed consistent values of grade, especially for (II), suggesting that the same ratio of graphite and LMOs report to the overflow throughout the length of the experiment. This phenomenon could be explained by the association of LMO and graphite particles, perhaps entrapped in the form of aggregates.

When kerosene was added during attrition (III), the mass pull increased to 49.2% and graphite recovery increased to 98.1%. Under such conditions, the energy input through the attrition pre-treatment improved the emulsification of the oily collector, likely promoting the reagent adsorption and subsequently improving particle-bubble attachment [44–46]. It was observed in Figure 4 that adding kerosene during attrition (III) increased as did the recovery of Co, Ni, and Mn compared to (II). While kerosene increased the graphite recovery, it also promoted the flotation of metallic particles, highlighting a non-selective character of the oily collector. In a previous study [35], it was observed that kerosene interacted with graphite particles as well as with lithium metal oxide particles, increasing their agglomeration and their attachment to an air bubble.

The improvement in the C grade between (I) and (II) is correlated with the decrease in the metals reporting to the overflow product (Figure 4). These metals belong to specific battery components. The main metals identified in the overflow product were Co, Mn, and Ni, and their grades decreased with the attrition pre-treatment from 9.4% to 5.1% for Co, 6.7% to 4.4% for Mn, and 3.9% to 3.3% for Ni. These elements are contained in the LMOs from the cathode electrode, which in this industrial black mass were a mixture of LCO and NMC. The LMOs can be coated with residual binder (e.g., PVDF), which will render them hydrophobic enough to be recovered by true flotation [23]. Therefore, the removal of binder by attrition seems to impact the LMO recovery, as will be further discussed in Section 3.2.

The other metals Al, Cu, and Fe had a low grade in the overflow product (i.e., <2%), which slightly decreased with attrition pre-treatment (Figure 4). The Cu particles likely originated from the anode electrode foil, which were well liberated from the graphite particles and the Fe element belonged to the casing particles, as discussed in the characterization study by Vanderbruggen et al. [43] of this black mass. Since Cu and Fe particles have a good wettability [46] and are free of binder, they are likely recovered by entrainment in the overflow product. Al particles are likely to be from the electrode foil since no Al-containing LMOs are expected in the black mass used in this study. The Al trend in (I) of increased recovery and grade after 1 min (corresponding to the fourth point in cumulative grade/recovery curves in Figure 4I) as similar to Co. A reasonable explanation for this similarity is that Al foil particles remained attached to LMOs in this case.

3.2. Possible Flotation Mechanisms as Result of Black Mass Pre-Treatment

To better understand the flotation behavior of the spent black mass and the effect of attrition pre-treatment, flotation tests with a model black mass were performed. Binder-free and fully liberated LMOs and graphite particles were used to approximate an ideal flotation behavior. In addition, to estimate the degree of entrainment, a glass tracer was added to the black mass used as feed.

3.2.1. Effect of Attrition on the PSD

The PSD results of the model black mass and spent black mass with and without attrition are displayed in Table 1.

Table 1. Attrition pre-treatment effect on the PSD of the model black mass and spent black mass.

Size (μm)	Model Black Mass		Spent Black Mass	
	Without Pre-Treatment	After Pre-Treatment	Without Pre-Treatment	After Pre-Treatment
D_{10}	10.7 ± 0.6	10.8 ± 0.6	2.7 ± 0.1	2.1 ± 0.1
D_{50}	18.0 ± 0.2	17.9 ± 0.2	16.9 ± 0.1	14.1 ± 0.3
D_{90}	27.1 ± 0.6	26.9 ± 0.1	53.1 ± 1.3	45.9 ± 1.5

For the model black mass, made of liberated LMOs and graphite particles (Figure 5), the attrition showed no effect on the PSD with similar D_{10}, D_{50}, and D_{90} for both samples (Table 1). Therefore, it is safe to assume that the attrition method used in this study does not damage the structure of individual particles of the electrode materials.
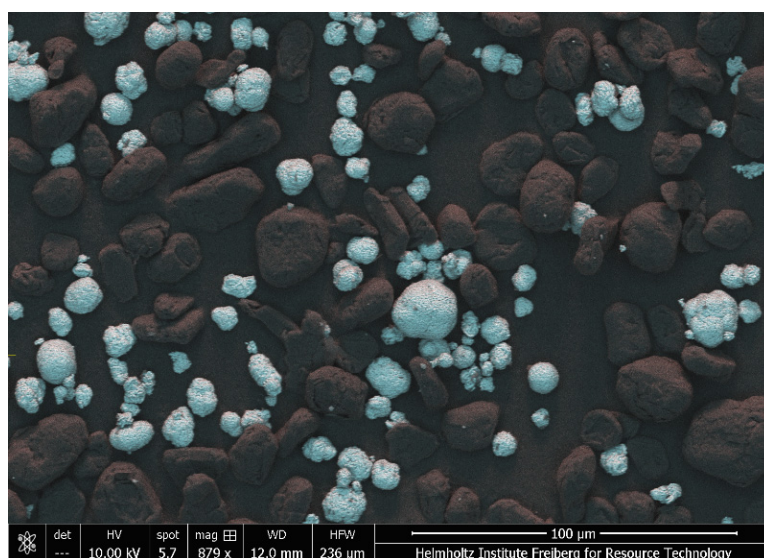
Figure 5. SEM image with imposed colors of the model black mass before attrition. LMO particles in blue and graphite particles in black.

The spent black mass had a coarser particle size distribution than the model black mass, with D_{90} of 53.1 μm and 27.1 μm, respectively. As observed in the SEM image (Figure 6), the graphite particles in the spent black mass appeared to be well liberated and with sizes similar to those in the model black mass. Consequently, the size differences between the model and spent black mass can be mainly associated with the LMOs that appear as aggregates formed with the aid of a PVDF binder. The fact that the PVDF binder was not fully decomposed after pyrolysis might be linked to the way that the batteries were treated to produce the black mass used in this study. In the industrial processing, batteries were not opened during vacuum pyrolysis, in contrast with publications from other groups, where the pyrolysis stage was conducted directly on black mass or on manually dismantled electrodes [13,47,48]. The compacted structure of the electrodes in the intact battery, in addition to the possibility of thermal gradient, may hinder the complete decomposition of the binder. On the other hand, the superior liberation degree of graphite particles compared with LMOs can be related to the weaker interaction between PVDF and graphite [49]. It is also possible that a different water soluble binder was used for the anode electrode (e.g., SBR-CMC) [50].
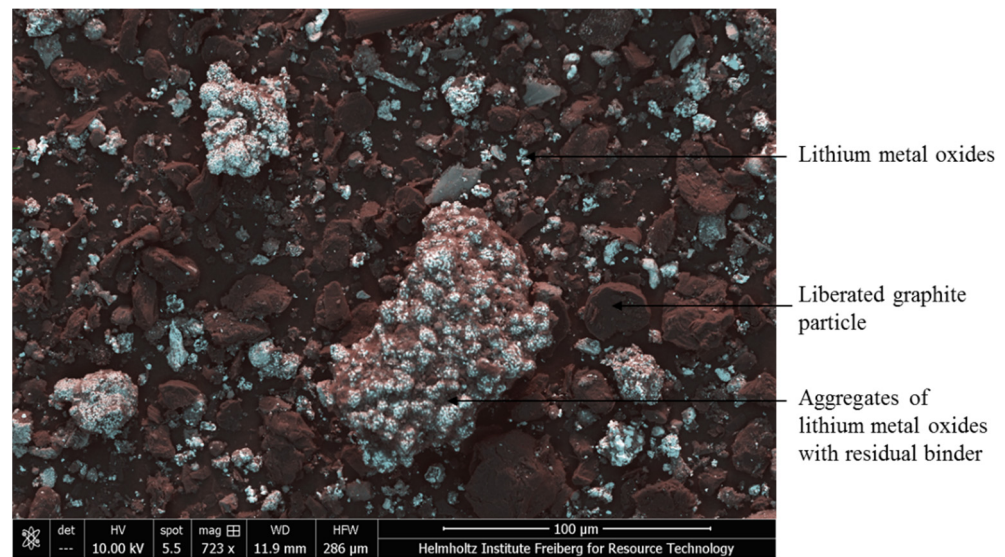
Figure 6. SEM image with imposed color of the spent black mass before attrition. The composition is represented by false color differences, blue was imposed for high atomic numbers (e.g., Co, Ni, Mn) and black for low atomic numbers (e.g., C, F).

It is also of note that the spent black mass presents a smaller D_{10} compared to the model black mass of 2.7 μm and 10.7 μm, respectively. These were evidently ultrafine products obtained during the comminution staged. Contrary to the attrition pre-treatment, the comminution stage is an energy intensive process that affects the structure of some active particles. Nevertheless, for this industrial black mass, the overall shape of the anode particles could be considered well conserved (Figure 6). The retention of the spheroidized shape of the graphite particles is a true advantage since it would allow for the reuse of these graphite particles for battery production, therefore decreasing the anode costs. Indeed, it is known that additional spheroidization may be resource intensive [51,52].

As observed in Table 1, 10 min of attrition pre-treatment reduces the PSD of the spent black mass, as some of the LMOs aggregates are de-agglomerated. This explanation is also confirmed by the study of Zhan et al. [53], who studied the de-agglomeration of cathode electrodes with a commercial blender. In their study, they delaminated the cathode active particles and found that 85% of these cathode active particles were coarser than 37 μm. They applied 20 min of high-shear forces on these cathode active particles, decreasing their PSD below 37 μm. As shown with the model black mass where the pristine structure of the LMOs was conserved after attrition of the model black mass, the size reduction in the case of the spent black mass was attributed to a de-agglomeration process due to the liberation of cathode composites from PVDF binders.

They concluded that the size of the cathode composites was effectively reduced upon a de-agglomeration process due to the liberation of cathode composites from PVDF binders. Attrition of black mass aids by detaching the coated binder, producing fine liberated binder particles as observed in the SEM image in Supplementary Materials (Figure S1).

3.2.2. Effect of Residual Binder on LMO Recovery

As seen in Section 3.1, the attrition pre-treatment reduced the LMO recovery in the overflow product. In this section, the recovery of LMOs due to the binder residual is discussed through the comparison of the model and spent black mass. The final recoveries obtained after 6.5 min in the overflow product are summarized in Figure 7.
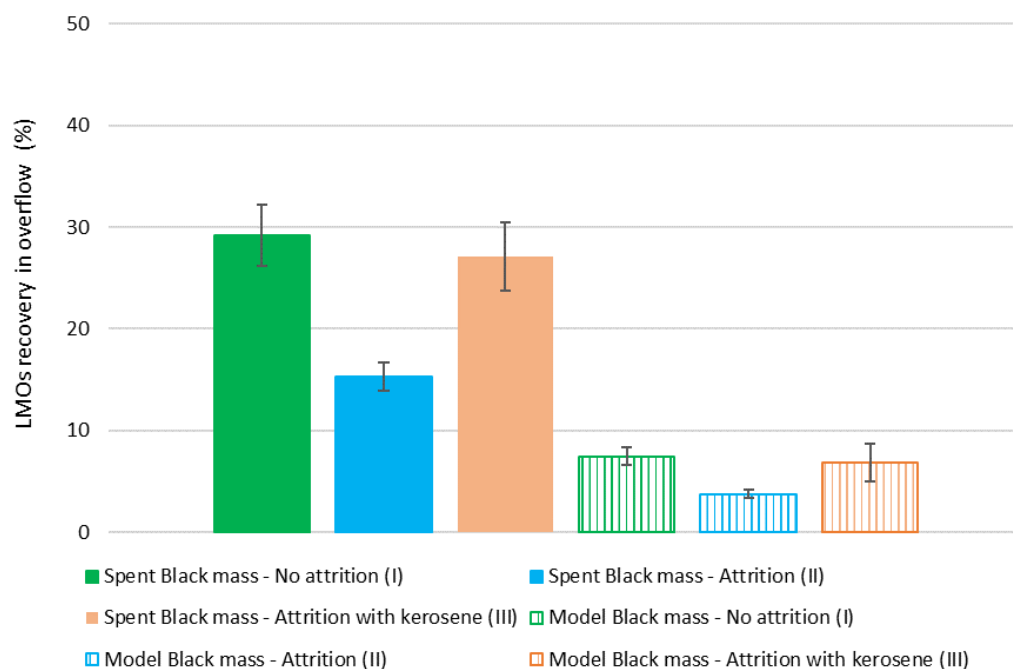
Figure 7. Recoveries of LMOs (including Co, Ni, and Mn elements) from spent black mass and model black mass with the different flotation flows: no attrition pre-treatment, with attrition pre-treatment, and attrition pre-treatment with kerosene. The results are average values of four experiments and the error bars represent an interval confidence of 90%.

For the spent pyrolyzed black mass, the LMO recovery in the overflow product was 29.2 ± 3% without attrition pre-treatment (I). This result is comparable to the flotation study of Zhang et al. [23], where they also used an oily collector and MIBC for the flotation, and recovered 36.5% of the LMOs from a crushed pyrolyzed spent black mass in the overflow product. According to the literature on black mass flotation studies, a minimum of 10% and up to 50% of LMOs reported to the overflow, depending on the recycling process applied and the amount of binder removed [15,23,24,54]. In most of these studies, it was assumed that the LMO recovery in the overflow product was due to true flotation via the residual binder, although our group has recently demonstrated that other mechanisms may be responsible for their flotation [35]. The significant difference in LMO recovery between the spent and model black mass (i.e., 29.2 ± 3% and 7.5 ± 0.9%, respectively) hereby measured (Figure 7) highlights the contribution of the residual binder in the LMO recovery. Moreover, the LMO recovery from the spent black mass dropped to 15.3 ± 1.4% when an attrition pre-treatment was applied. This decrease in LMO recovery can be connected to the removal of residual binder and the deagglomeration of LMOs, as discussed in Section 3.2.1.

As observed in Figure 8, the flotation kinetics of LMOs were different between the spent black and model black mass. For the model black mass, most of the LMOs were recovered within 18 s from the start of flotation. For the spent black mass, only 25% of the total recovered LMOs were collected within such a timeframe. Moreover, the LMO kinetics showed two regimes, with an inflexion point at ca. 90 s. Compared to the model black mass, the spent black mass contained LMO particles coated with residual binder, which may be recovered through true flotation, explaining the differences in kinetic behaviors.
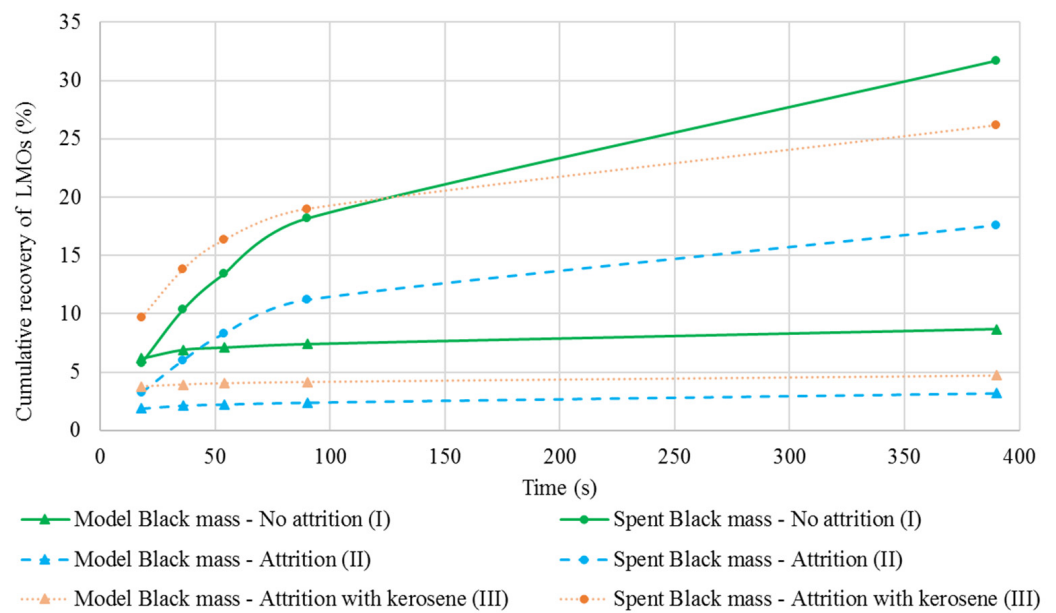
Figure 8. Recovery of the LMOs from spent black mass and model black mass in the overflow product according to the flotation time.

Kinetics also are influenced by the conditioning procedure. When the collector is added during the attrition pre-treatment (III), more LMOs were recovered at the beginning of flotation compared to (I) for both systems, highlighting that such collector effectively enhances hydrophobicity in a non-selective manner. As shown in the research of Vanderbruggen et al. (2021) [37], kerosene increased the attachment probability of LMO particles to an air bubble. During attrition pre-treatment (III), some of the residual binders may have been partially removed, nevertheless resulting in a relatively similar LMO recovery than without attrition of $27.1 \pm 3.4\%$ (III) and $29.2 \pm 3\%$ (I), respectively. Still, it was higher compared to attrition alone (II), which might be a result of enhanced dispersion of kerosene droplets in the presence of high shear (16,000 rpm). As explained by Hornn et al. [55], during agitation, the oil droplets are split by shear force, decreasing the size of the droplets and increasing the number of droplets in the pulp. Consequently, the collision and attachment of LMOs and fine oil droplets during the attrition stage was increased.

The results with the model black mass showed that the effect of attrition went beyond the residual binder. Even without the residual binder, the LMO recovery decreased with attrition pre-treatment from $7.5 \pm 0.9\%$ to $3.8 \pm 0.5\%$, suggesting that other mechanisms than true flotation through the binder are occurring during black mass flotation.

As shown in Figure 9, the graphite kinetics of the spent black mass (I) and (II) were similar, suggesting that attrition does not seem to influence the graphite kinetics compared to the LMO kinetics (Figure 8). The kinetics of spent graphite were slower than fresh graphite from the model black mass, with 58.3% and 77.9% of graphite recovery at 90 s, respectively, without attrition (I). This difference of kinetics can be associated with the graphite hydrophobicity, as explained in Section 3.1. The addition of kerosene during attrition pre-treatment (III) improved the kinetics of graphite for both the spent black mass and model black mass.
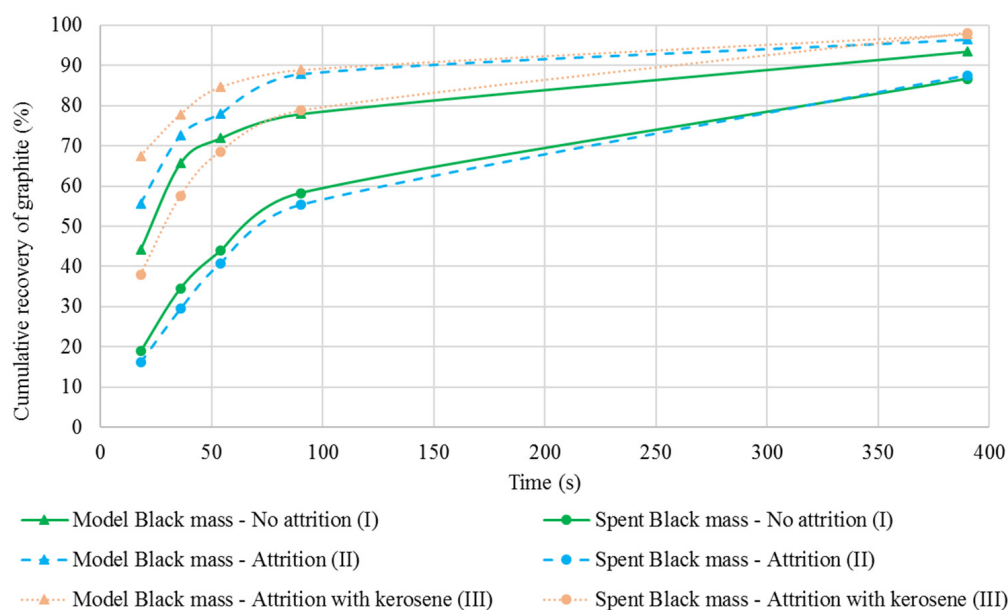
Figure 9. Carbon recovery from the spent black mass and model black mass in the overflow product according to the flotation time.

3.2.3. Black Mass and Particle Entrainment

Entrainment is a common phenomenon in flotation in which a nonselective recovery occurs, thus having a negative impact on the overflow product grade. To study the entrainment degree of the spent and model black mass, an entrainment tracer consisting of fine hydrophilic particles was added to the flotation feed. As the tracer is considered fully hydrophilic, it was assumed that it could only be recovered through entrainment. In addition, the tracer particles being lighter (tracer particle density of 2.5 g/cm^3 vs. NMC particle density of 4.6 g/cm^3) and finer (D$_{90}$ 8 μm vs. 20 μm) [56], they should present a higher probability to be entrained than the LMO particles. ENT of the tracer and LMOs after 18 s, 36 s, 54 s, 90 s, and 390 s calculated for each system with Equation (2) are summarized in Table 2. The data used for the calculation are provided in Supplementary Materials (Table S1).

Table 2. Entrainment degree of the tracer particles and the LMO particles for the spent black mass and model black mass.

Conditioning	No Attrition (I)		Attrition (II)		Attrition with Kerosene (III)	
			Spent Black mass			
Cumulative time (s)	R/W LMOs	ENT Tracer	R/W LMOs	ENT Tracer	R/W LMOs	ENT Tracer
18	3.30	0.71	1.86	0.59	2.34	1.22
36	3.15	0.69	2.42	0.73	2.25	1.01
54	2.99	0.64	2.28	0.67	2.25	0.93
90	3.00	0.64	2.15	0.60	2.25	0.86
390	2.44	0.55	1.47	0.46	1.84	0.67
			Model Black mass			
Cumulative time (s)	R/W LMOs	ENT Tracer	R/W LMOs	ENT Tracer	R/W LMOs	ENT Tracer
18	1.10	0.47	0.61	0.51	0.90	0.80
36	1.01	0.42	0.53	0.46	0.83	0.74
54	0.99	0.41	0.51	0.44	0.78	0.70
90	0.95	0.39	0.46	0.42	0.74	0.68
390	0.67	0.29	0.30	0.28	0.58	0.50

It is important to highlight that the values in Table 2 for LMOs in the spent black mass include the recovery by all possible flotation mechanisms, either aided by residual

binder (as discussed in Section 3.2.2.), entrapment within hydrophobic agglomerates, or entrainment. This explains the high difference between the LMOs in the spent black mass compared to the model black mass (e.g., 2.64 vs. 0.64 for (I)). Thus, the entrainment degree and R/W only give an indication of the behavior of the particles during flotation, and the values between the two systems should not be directly compared, although trends can be identified with each specific set of flotation conditions. It was observed (Table 2) that the ENT degree of the tracer was similar for the model black mass (I) and (II), suggesting that both systems present similar entrainment probability. In addition, when attrition was applied, the ENT degree of the LMOs and tracer were similar (II), highlighting that the LMO particles were mainly recovered by entrainment mechanisms. However, the values of ENT and R/W differed between (I) and (II) by 0.67 and 0.30, respectively. This result for the model black mass suggests that there are additional mechanisms other than entrainment in promoting LMO recovery.

For instance, when the model or spent black mass is added to water, non-wetted clusters were observed on top of the pulp, as shown in Supplementary Material (Figure S2), some of which were not broken even under a rotor agitation at 1000 min^{-1}. As shown in the study of Vanderbruggen et al. [35], LMO particles were entrapped in such non-wetted clusters. By applying an attrition pre-treatment, such unselective agglomerates were broken [57] and the full wetting of LMOs in the pulp was promoted. This is highlighted by the decrease in the LMO entrainment degree in the model black mass between (I) and (II). However, this effect was diminished when kerosene was added during attrition, as shown by our group Vanderbruggen et al. [35] and others Guan et al. [58], where kerosene enhanced agglomeration, resulting in LMO entrapment. These results suggest that the collector addition step has a strong impact on the entrainment of the impurities in the overflow product.

The possible effects of attrition pre-treatment are summarized in Figure 10. Attrition pre-treatment removes a part of the residual binder, reducing the true flotation of the spent LMOs (Figure 10, on the right). In addition, one hypothesis is the disaggregation and full wetting of the particles during attrition (Figure 10, on the left), which would explain the decrease in LMO recovery for the model black mass.
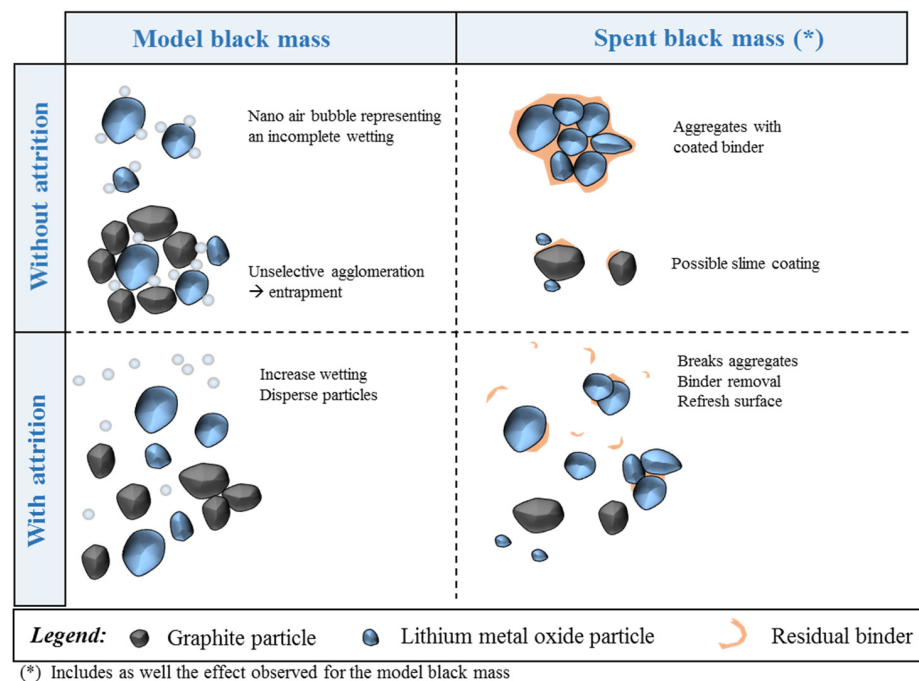

Figure 10. Summary of the potential effects of attrition on the black mass. (*) the effects observed in the model black mass are also included in the spent black mass.

4. Conclusions

The efficient separation of LMOs and graphite from spent LIBs by flotation is a challenging research topic due to the complexity of the black mass composition. The spent black mass studied in this work was composed of ultrafine and coarse aggregates of LMOs (Co, Ni, Mn) with residual binders, liberated graphite particles, and impurities such as Cu and Al from the electrode foils. Two reagents were used for the black mass flotation tests: an oily collector and a frother, (i.e., kerosene and MIBC, respectively). It was found that even though graphite is naturally hydrophobic, a collector is necessary to enhance the hydrophobicity of spent graphite, likely due to the modification of its surface during the battery lifetime (e.g., binder adhesion or SEI layer formation) and recycling process (e.g., pyrolysis, oxidation).

More than 85% of the spent graphite is recoverable if enough collector is used, leading to a cathode-rich underflow product, with less than 3% C grade. A main challenge for the LMO/graphite separation by flotation is the recovery of LMOs in the overflow product mainly due to two mechanisms: true flotation promoted by a coating of residual binder and entrainment. An attrition pre-treatment with high shear forces was tested to reduce both phenomena.

The results underline that the kerosene is a non-selective collector enhancing the flotation of both graphite and LMOs, especially when it is introduced during the attrition pre-treatment step. Most of the LMO recovery from spent black mass can be reasonably attributed to true flotation aided by the residual binder coating on the LMO particles. The attrition pre-treatment is efficient at removing part of the binder and decreasing the LMO recovery by refreshing the surface of such particles and by breaking LMO aggregates. This study also shows that part of the LMOs was recovered by entrainment and that attrition reduced the entrapment of LMOs.

It was shown that conditioning black mass with an attrition pre-treatment step promotes a better separation of graphite and LMOs by flotation. This improvement in separation efficiency is of interest since it creates two valuable products: an LMO product with a high grade of metals that could be easily treated for battery remanufacturing or further refined by hydrometallurgical means, and a spheroidized graphite concentrate that can be further purified to remove the fine metal impurities and be re-used in new batteries as an anode material. With this step, the LIB recycling processes would move closer to the circular economy objective of closing the loop for raw materials.

References

1. Jenu, S.; Deviatkin, I.; Hentunen, A.; Myllysilta, M.; Viik, S.; Pihlatie, M. Reducing the climate change impacts of lithium-ion batteries by their cautious management through integration of stress factors and life cycle assessment. *J. Energy Storage* **2020**, *27*, 101023. [CrossRef]
2. Global Battery Alliance. *A Vision for a Sustainable Battery Value Chain in 2030*; Unlocking the Full Potential to Power Sustainable Development and Climate Change Mitigation; Report from World Economic Forum: Geneva, Switzerland, 2019.
3. Moradi, B.; Botte, G.G. Recycling of graphite anodes for the next generation of lithium ion batteries. *J. Appl. Electrochem.* **2016**, *46*, 123–148. [CrossRef]
4. Porvali, A.; Aaltonen, M.; Ojanen, S.; Velazquez-Martinez, O.; Eronen, E.; Liu, F.; Wilson, B.P.; Serna-Guerrero, R.; Lundström, M. Mechanical and hydrometallurgical processes in HCl media for the recycling of valuable metals from Li-ion battery waste. *Resour. Conserv. Recycl.* **2019**, *142*, 257–266. [CrossRef]
5. Larouche, F.; Tedjar, F.; Amouzegar, K.; Houlachi, G.; Bouchard, P.; Demopoulos, G.P.; Zaghib, K. Progress and Status of Hydrometallurgical and Direct Recycling of Li-Ion Batteries and Beyond. *Materials* **2020**, *13*, 801. [CrossRef]
6. Or, T.; Gourley, S.W.D.; Kaliyappan, K.; Yu, A.; Chen, Z. Recycling of mixed cathode lithium-ion batteries for electric vehicles: Current status and future outlook. *Carbon Energy* **2020**, *2*, 6–43. [CrossRef]
7. Halleux, V. *New EU Regulatory Framework for Batteries—Setting Sustainability Requirements*; European Parliamentary Research Service: Brussels, Belgium, 2021.
8. Asenbauer, J.; Eisenmann, T.; Kuenzel, M.; Kazzazi, A.; Chen, Z.; Bresser, D. The success story of graphite as a lithium-ion anode material-fundamentals, remaining challenges, and recent deveelopments including silicon (oxide) composites. *Sustain. Energy and Fuels* **2020**, *4*, 5387–5416. [CrossRef]
9. Gaines, L.; Sullivan, J.L.; Burnham, A. Life-Cycle Analysis for Lithium-Ion Battery Production and Recycling. In Proceedings of the 90th Annual Meeting of the Transportation Research Board, Washington, DC, USA, 23–27 January 2011.
10. Blengini, G.A.; Nuss, P.; Dewulf, J.; Nita, V.; Peirò, L.T.; Vidal-Legaz, B.; Latunussa, C.; Mancini, L.; Blagoeva, D.; Pennington, D.; et al. EU methodology for critical raw materials assessment: Policy needs and proposed solutions for incremental improvements. *Resour. Policy* **2017**, *53*, 12–19. [CrossRef]
11. Damm, S.; Qizhong, Z. *Supply and Demand of Natural Graphite—DERA Rohstoffinformationen*; Federal Institute for Geosciences and Natural Resources (BGR), German Mineral Resources Agency (DERA): Berlin, Germany, 2021.
12. Werner, D.; Peuker, U.A.; Mütze, T. Recycling chain for spent lithium-ion batteries. *Metals* **2020**, *10*, 316. [CrossRef]
13. Zhan, R.; Yang, Z.; Bloom, I.; Pan, L. Significance of a Solid Electrolyte Interphase on Separation of Anode and Cathode Materials from Spent Li-Ion Batteries by Froth Flotation. *ACS Sustain. Chem. Eng.* **2021**, *9*, 531–540. [CrossRef]
14. Kim, Y.; Matsuda, M.; Shibayama, A.; Fujita, T. Recovery of LiCoO$_2$ from Wasted Lithium Ion Batteries by using Mineral Processing Technology. *Resour. Process.* **2003**, *51*, 3–7. [CrossRef]
15. Zhan, R.; Oldenburg, Z.; Pan, L. Recovery of active cathode materials from lithium-ion batteries using froth flotation. *Sustain. Mater. Technol.* **2018**, *17*, e00062. [CrossRef]
16. Zhang, G.; Du, Z.; He, Y.; Wang, H.; Xie, W.; Zhang, T. A sustainable process for the recovery of anode and cathode materials derived from spent lithium-ion batteries. *Sustainability* **2019**, *11*, 2363. [CrossRef]
17. Shin, H.; Zhan, R.; Dhindsa, K.S.; Pan, L.; Han, T. Electrochemical Performance of Recycled Cathode Active Materials Using Froth Flotation-based Separation Process. *J. Electrochem. Soc.* **2020**, *167*, 020504. [CrossRef]
18. Gaines, L.; Dai, Q.; Vaughey, J.T.; Gillard, S. Direct recycling R&D at the recell center. *Recycling* **2021**, *6*, 31.
19. Rothermel, S.; Evertz, M.; Kasnatscheew, J.; Qi, X.; Grützke, M.; Winter, M.; Nowak, S. Graphite Recycling from Spent Lithium-Ion Batteries. *ChemSusChem* **2016**, *9*, 3473–3484. [CrossRef] [PubMed]
20. De Meatza, I.; Bengoechea, M.; Eguia-Barrio, I.; Tedjar, F.; Cognard, J.; Vieira Carvalho, D.; Moretti, A.; Passerini, S. Enhancing lithium-ion battery recycling: Evaluation of graphite and carbon recovered from aged cells for the production of 'new' negative electrodes. In Proceedings of the 7th Transport Research Arena TRA 2018, Vienna, Austria, 16–19 April 2018.
21. Wills, B.A.; Finch, J.A. Chapter 12—Froth Flotation. In *Wills' Mineral Processing Technology*, 8th ed.; Wills, B.A., Finch, J.A., Eds.; Butterworth-Heinemann: Boston, MA, USA, 2016; pp. 265–380.
22. Chelgani, S.C.; Rudolph, M.; Kratzsch, R.; Sandmann, D.; Gutzmer, J. A Review of Graphite Beneficiation Techniques. *Miner. Process. Extr. Metall. Rev.* **2016**, *37*, 58–68. [CrossRef]
23. Zhang, G.; He, Y.; Wang, H.; Feng, Y.; Xie, W.; Zhu, X. Removal of Organics by Pyrolysis for Enhancing Liberation and Flotation Behavior of Electrode Materials Derived from Spent Lithium-Ion Batteries. *ACS Sustain. Chem. Eng.* **2020**, *8*, 2205–2214. [CrossRef]
24. Yu, J.; He, Y.; Ge, Z.; Li, H.; Xie, W.; Wang, S. A promising physical method for recovery of LiCoO$_2$ and graphite from spent lithium-ion batteries: Grinding flotation. *Sep. Pur.* **2018**, *190*, 45–52. [CrossRef]
25. He, Y.; Zhang, T.; Wang, F.; Zhang, G.; Zhang, W.; Wang, J. Recovery of LiCoO$_2$ and graphite from spent lithium-ion batteries by Fenton reagent-assisted flotation. *J. Clean. Prod.* **2017**, *143*, 319–325. [CrossRef]
26. Yu, J.; He, Y.; Li, H.; Xie, W.; Zhang, T. Effect of the secondary product of semi-solid phase Fenton on the flotability of electrode material from spent lithium-ion battery. *Powder Technol.* **2017**, *315*, 139–146. [CrossRef]
27. Zhang, C.; Song, J.; Zhang, J.; Zhang, J.; Xing, J.; Hu, D.; Peng, Y.; Zhou, J.; Liu, Q.; Gu, H.; et al. Understanding and application of an electroplating sludge-derived catalyst with an active texture for improved NO reduction. *Sci. Total Environ.* **2018**, *631–632*, 308–316. [CrossRef] [PubMed]

28. Zhang, G.; Ding, L.; Yuan, X.; He, Y.; Wang, H.; He, J. Recycling of electrode materials from spent lithium-ion battery by pyrolysis-assisted flotation. *J. Environ. Chem. Eng.* **2021**, *9*, 106777. [CrossRef]

29. Zhang, G.; He, Y.; Wang, H.; Feng, Y.; Xie, W.; Zhu, X. Application of mechanical crushing combined with pyrolysis-enhanced flotation technology to recover graphite and LiCoO2 from spent lithium-ion batteries. *J. Clean. Prod.* **2019**, *231*, 1418–1427. [CrossRef]

30. Wang, L.; Peng, Y.; Runge, K.; Bradshaw, D. A Review of Entrainment: Mechanisms, Contributing Factors and Modelling in Flotation. *Miner. Eng.* **2015**, *70*, 77–91. [CrossRef]

31. Smith, P.G.; Warren, L.J. Entrainment of Particles into Flotation Froths. *Miner. Process. Extr. Met. Rev.* **2007**, *5*, 123–145. [CrossRef]

32. Kursun, H. Effect of fine particles' entrainment on conventional and column flotation. *Part. Sci. Technol.* **2014**, *32*, 251–256. [CrossRef]

33. Yang, B.; Yin, W.; Zhu, Z.; Wang, D.; Han, H.; Fu, Y.; Sun, H.; Chu, F.; Yao, J. A new model for the degree of entrainment in froth flotation based on mineral particle characteristics. *Powder Technol.* **2019**, *354*, 358–368. [CrossRef]

34. Hoang, D.H.; Kupka, N.; Peuker, U.A.; Rudolph, M. Flotation study of fine grained carbonaceous sedimentary apatite ore – Challenges in process mineralogy and impact of hydrodynamics. *Miner. Eng.* **2018**, *121*, 196–204. [CrossRef]

35. Vanderbruggen, A.; Sygusch, J.; Rudolph, M.; Serna-guerrero, R. A contribution to understanding the flotation behavior of lithium metal oxides and spheroidized graphite for lithium-ion battery recycling. *Colloids Surf. A Physicochem. Eng. Asp.* **2021**, *626*, 127111. [CrossRef]

36. Chen, G.; Grano, S.; Sobieraj, S.; Ralston, J. Effect of high intensity conditioning on the flotation of a nickel ore. Part 1: Size-by-size analysis. *Miner. Eng.* **1999**, *12*, 1185–1200. [CrossRef]

37. Lu, X.; Forssberg, E. Technical note flotation selectivity and upgrading of Woxna fine graphite concentrate. *Miner. Eng.* **2001**, *14*, 1541–1543. [CrossRef]

38. Sun, W.; Deng, M.J.; Hu, Y.H. Fine particle aggregating and flotation behavior induced by high intensity conditioning of a CO$_2$ saturation slurry. *Min. Sci. Technol.* **2009**, *19*, 483–488. [CrossRef]

39. Sun, Y.; Xie, G.; Peng, Y.; Chen, Y.; Ma, G. How Does High Intensity Conditioning Affect Flotation Performance? *Int. J. Coal Prep. Util.* **2019**, *39*, 302–316. [CrossRef]

40. Zhou, S.; Wang, X.; Bu, X.; Shao, H.; Hu, Y.; Alheshibri, M.; Li, B.; Ni, C.; Peng, Y.; Xie, G. Effects of emulsified kerosene nanodroplets on the entrainment of gangue materials and selectivity index in aphanitic graphite flotation. *Miner. Eng.* **2020**, *158*, 106592. [CrossRef]

41. Ruismäki, R.; Rinne, T.; Dańczak, A.; Taskinen, P.; Serna-Guerrero, R.; Jokilaakso, A. Integrating Flotation and Pyrometallurgy for Recovering Graphite and Valuable Metals from Battery Scrap. *Metals* **2020**, *10*, 680. [CrossRef]

42. Vanderbruggen, A.; Gugala, E.; Blannin, R.; Bachmann, K.; Serna-Guerrero, R.; Rudolph, M. Automated mineralogy as a novel approach for the compositional and textural characterization of spent lithium-ion batteries. *Miner. Eng.* **2021**, *169*, 106924. [CrossRef]

43. Johnson, N.W. The Flotation Behaviour of Some Chalcopyrite Ores. Ph.D. Thesis, University of Queensland, Brisbane, Australia, 1972.

44. Feng, D.; Aldrich, C. Effect of preconditioning on the flotation of coal. *Chem. Eng. Commun.* **2005**, *192*, 972–983. [CrossRef]

45. Wang, H.; Yang, W.; Li, D.; Zhang, C.; Yan, X.; Wang, L.; Zhang, H. Enhancement of coal flotation using impact flow conditioning pulp. *J. Clean. Prod.* **2020**, *267*, 122124. [CrossRef]

46. Sheng, Y.; Fell, C.R.; Son, Y.K.; Metz, B.M.; Jiang, J.; Church, C.B. Effect of Calendering on Electrode Wettability in Lithium-Ion Batteries. *Front. Energy Res.* **2014**, *2*, 56. [CrossRef]

47. Li, W.; Yang, S.; Liu, N.; Chen, Y.; Xi, Y.; Li, S.; Jie, Y.; Hu, F. Study on Vacuum Pyrolysis Process of Cathode Sheets from Spent Lithium-ion Batteries. In *Minerals, Metals and Materials Series*; Springer International Publishing: Berlin/Heidelberg, Germany, 2019; pp. 421–435.

48. Wang, F.; Zhang, T.; He, Y.; Zhao, Y.; Wang, S.; Zhang, G.; Zhang, Y.; Feng, Y. Recovery of valuable materials from spent lithium-ion batteries by mechanical separation and thermal treatment. *J. Clean. Prod.* **2018**, *185*, 646–652. [CrossRef]

49. Widijatmoko, S.D.; Gu, F.; Wang, Z.; Hall, P. Selective liberation in dry milled spent lithium-ion batteries. *Sustain. Mater. Technol.* **2020**, *23*, e00134. [CrossRef]

50. Bresser, D.; Buchholz, D.; Moretti, A.; Varzi, A.; Passerini, S. Alternative binders for sustainable electrochemical energy storage-the transition to aqueous electrode processing and bio-derived polymers. *Energy Environ. Sci.* **2018**, *11*, 3096–3127. [CrossRef]

51. Frey, C. Processing of Natural Flake Graphite for Lithium-Ion-Batteries. In Proceedings of the EMPRC 2018, Essen, Germany, 15–26 June 2018; pp. 203–210.

52. Mundszinger, M.; Farsi, S.; Rapp, M.; Golla-Schindler, U.; Kaiser, U.; Wachtler, M. Morphology and texture of spheroidized natural and synthetic graphites. *Carbon N. Y.* **2017**, *111*, 764–773. [CrossRef]

53. Zhan, R.; Payne, T.; Leftwich, T.; Perrine, K.; Pan, L. De-agglomeration of cathode composites for direct recycling of Li-ion batteries. *Waste Manag.* **2020**, *105*, 39–48. [CrossRef] [PubMed]

54. Zhang, G.; He, Y.; Feng, Y.; Wang, H.; Zhu, X. Pyrolysis-Ultrasonic-Assisted Flotation Technology for Recovering Graphite and LiCoO$_2$ from Spent Lithium-Ion Batteries. *ACS Sustain. Chem. Eng.* **2018**, *6*, 10896–10904. [CrossRef]

55. Hornn, V.; Ito, M.; Shimada, H.; Tabelin, C.B.; Jeon, S.; Park, I.; Hiroyoshi, N. Agglomeration-Flotation of Finely Ground Chalcopyrite and Quartz: Effects of Agitation Strength during Agglomeration Using Emulsified Oil on Chalcopyrite. *Minerals* **2020**, *10*, 380. [CrossRef]

56. Wang, L.; Peng, Y.; Runge, K. Entrainment in froth flotation: The degree of entrainment and its contributing factors. *Powder Technol.* **2015**, *288*, 202–211. [CrossRef]

57. Song, S.; Lu, S. Theory and Applications of Hydrophobic Flocculation Technology. In *Developments in Mineral Processing, Proceedings of the XXI International Mineral Processing Congress, Rome, Italy, 23–27 July 2000*; Massacci, P., Ed.; Elsevier: Amsterdam, The Netherlands, 2000; Volume 13, pp. C5-31–C5-38.

58. Guan, W.; Sha, J.; Liu, P.; Peng, Y.; Xie, G. Effect of stirring time on oil agglomeration of fine coal. *J. South. Afr. Inst. Min. Metall.* **2018**, *118*, 89–94. [CrossRef]